# Few-Shot Closed-Loop Neural System Identification via Meta-Learning

**Anonymous authors**
**Paper under double-blind review**

## Abstract

We study few-shot closed-loop neural system identification in a meta-learning setting, where related source systems are used to learn a neural-network-based open-loop dynamics model for a new target system from limited feedback-controlled data. In closed loop, inputs are generated through output feedback; consequently, the observed trajectories are shaped by both the plant dynamics and the controller. Under feedback-dependent data generation and scarce target data, existing system identification methods are insufficient for recovering the open-loop dynamics. Based on meta-learning and neural closed-loop identification, we propose Meta-ICI, which learns an initialization for an intermediate operator to recover open-loop dynamics from limited target closed-loop data. We further extend Meta-ICI to fragmented target adaptation, where only scattered one-step transitions are available instead of continuous trajectories. This extension yields Fast Meta-ICI for fully observable systems, using fragmented transitions to support accurate long-horizon rollouts. To instantiate Fast Meta-ICI, we design a Schur-Koopman model that enforces the latent spectral-radius constraint during unconstrained optimization. Experiments on partially observable Liénard systems and fully observable nonlinear pendulum systems show that Meta-ICI improves few-shot adaptation and Fast Meta-ICI enables non-divergent long-horizon rollouts from fragmented target data.

## 1 Introduction

Dynamics models serve as a core component of modern machine learning systems for sequential decision making, including model-based reinforcement learning (Chua et al., 2018), model predictive control (Zhou et al., 2025), robotics (Kaufmann et al., 2023), and sequential time-series modeling (Chen et al., 2018). To successfully drive these decision-making processes, models cannot merely fit passively logged trajectories; they must actively support rollouts, planning, and counterfactual predictions. Specifically, the model should predict how the system would evolve under input sequences or excitation distributions different from those observed during data collection (Chua et al., 2018; Zhou et al., 2025). Neural-network-based dynamics models provide data-driven and differentiable parameterizations for this purpose, making them highly useful when first-principles models are unavailable, incomplete, or insufficiently accurate (Pillonetto et al., 2025).

In practice, obtaining the ideal data for learning such a model is often difficult. Many physical systems cannot be freely excited in open loop because they must remain stabilized by an existing feedback policy, or controller (Forssell & Ljung, 1999). Even under feedback control, informative identification experiments can be costly, as excitation signals consume operating time and may perturb the system away from normal operation (Ljung, 1998). Consequently, the available data for a target system may be limited, noisy, short, or fragmented rather than consisting of long continuous trajectories. This leads to the practical problem of few-shot closed-loop system identification, where the goal is to recover the open-loop dynamics of the plant from a small amount of feedback-controlled data.

Few-shot closed-loop system identification is more difficult than standard few-shot dynamics learning. Standard squared prediction-error training implicitly assumes that the prediction noise is orthogonal to the variables used by the predictor. In closed-loop settings, this condition is generally violated because the input

sequence is generated through feedback from noisy observations, making the input statistically coupled with disturbances and measurement noise (Dinkla et al., 2026). As a result, directly minimizing prediction error on closed-loop trajectories can yield a biased estimate of the plant dynamics. The few-shot setting further amplifies this issue, since only a small amount of target data is available to adapt a neural network and distinguish plant-specific dynamics from feedback-induced correlations.

Closed-loop identification methods explicitly account for the feedback mechanism instead of treating feedback-controlled trajectories as ordinary supervised data (Srivastava et al., 2023; Zhu et al., 2021; Boroujeni et al., 2025). In particular, Internal Controller Identification (ICI) reformulates closed-loop system identification as the learning of a stable internal operator associated with the known controller (Boroujeni et al., 2025). This provides a way to address feedback-induced bias, but ICI is trained for each target system independently and requires sufficiently informative target-system data. Meta-learning provides a way to address this limitation by using related source systems to learn a transferable initialization (Chakrabarty et al., 2023; 2025; Clavera et al., 2019).

Motivated by the complementary roles of ICI and meta-learning, we propose Meta-ICI, a framework that meta-learns the initialization of an ICI-compatible internal operator across related closed-loop systems. The ICI structure accounts for the feedback mechanism and mitigates feedback-induced bias, while meta-learning enables the operator to be adapted from limited target data rather than trained independently from scratch. For a new target system, the adapted internal operator is converted into the corresponding open-loop dynamics through the ICI reparameterization. Because ICI is formulated in terms of input-output operators, Meta-ICI can also be instantiated with recurrent stable architectures for partially observable systems.

For fully observable systems, we further develop Fast Meta-ICI, which exploits the Markov property of the observed state. In this case, target adaptation can only use scattered one-step transitions rather than long contiguous trajectories, but the learned model still supports long-horizon counterfactual rollouts. Fast Meta-ICI addresses this mismatch by combining a Schur-Koopman (SK) architecture with a hybrid step-wise/sequence-wise objective based on MAML (Finn et al., 2017). The SK architecture provides a stable neural operator suitable for ICI, while the hybrid objective adapts from fragmented one-step data and meta-optimizes rollout accuracy.

Our contributions are summarized as follows.

1. We introduce few-shot closed-loop neural system identification as a meta-learning problem, where the goal is to recover open-loop dynamics from limited feedback-controlled data by leveraging related source systems. To the best of our knowledge, this is among the first attempts to study meta-learning for closed-loop system identification.

2. We propose Meta-ICI, a model-agnostic meta-learning framework for ICI-compatible stable neural operators. Meta-ICI transfers the initialization of the internal operator used by ICI, enabling adaptation from limited closed-loop data while preserving the closed-loop identification structure needed to address feedback-induced bias.

3. For fully observable systems, we design an ICI-compatible SK operator with a built-in spectral-radius constraint. The operator uses a Koopman-inspired latent linear representation and a Schur parameterization to preserve stability constraints during unconstrained gradient-based optimization, making it compatible with standard optimizers such as SGD and Adam. Moreover, we prove that, under the stated latent contraction and reconstruction-consistency assumptions, this architecture defines a finite-gain $\mathcal{L}_p$-stable operator.

4. We propose a hybrid meta-learning objective for Fast Meta-ICI that turns fragmented target data into rollout-oriented adaptation. Instead of requiring continuous target trajectories, the inner loop adapts from scattered one-step transitions. The outer loop then optimizes the post-adaptation model through multi-step rollouts, enabling the learned initialization to support long-horizon counterfactual prediction.

5. We empirically validate the proposed methods on partially observable Liénard systems and fully observable nonlinear pendulum systems. The results show that Meta-ICI substantially improves few-shot adaptation

over scratch training, and that Fast Meta-ICI produces non-divergent long-horizon rollouts under shifted input distributions, approaching the corresponding full-data reference performance.

## 2 Related Work

**Deep neural networks for system identification.** Deep neural networks have been widely studied as flexible model classes for nonlinear system identification. Pillonetto et al. (2025) provide a recent survey of deep networks for system identification, covering various architectures as well as the optimization and regularization issues that arise when fitting dynamic models from input-output data. Beintema et al. (2023) proposed SUBNET for continuous-time nonlinear state-space identification, using a neural encoder to estimate latent initial states from subsequences and short simulations to approximate the full simulation loss. Control-oriented applications have also adopted neural predictors as system identification modules. For example, Frison & Gölzhäuser (2024) use Transformer-LSTM architectures for building heating system identification and forecasting. For feedback-controlled data, Boroujeni et al. (2025) provide a neural closed-loop identification framework by reformulating the problem as the learning of a stable internal operator associated with the known controller. However, both conventional deep-network-based identification methods and ICI are typically trained for each target system independently and require sufficiently informative target-system data. In contrast, our work studies few-shot adaptation across related feedback-controlled systems by meta-learning the initialization of ICI-compatible operators.

**Meta-learning for system identification.** Meta-learning has recently been explored as a way to improve data efficiency in neural system identification by leveraging data from related systems. Chakrabarty et al. (2023) proposed one of the first gradient-based meta-learning frameworks for neural state-space identification, using MAML to learn an initialization from similar source systems that can be rapidly adapted to a new target system with limited data. This work focused on autonomous neural state-space models and demonstrated advantages over supervised learning and transfer learning under limited target data. Chakrabarty et al. (2025) extended this direction to physically constrained neural system identification, incorporating domain-specific constraints into neural state-space models and demonstrating few-shot adaptation on real-world case studies. Besides, Rufolo et al. (2025) introduced a distributionally robust meta-learning objective that prioritizes high-loss tasks, improving worst-case and out-of-distribution performance. Forgione et al. (2025) proposed manifold meta-learning, which learns a low-dimensional manifold in the parameter space of an over-parameterized neural network to reduce adaptation complexity while preserving expressive power. These works show that meta-learning is a promising tool for few-shot neural system identification. However, they are primarily developed for open-loop trajectory data, and do not address closed-loop identification. Our work extends this line by meta-learning ICI-compatible operators, enabling few-shot adaptation to recover open-loop dynamics from feedback-controlled data.

**Stable neural operators and stable dynamics models.** Stability constraints have been widely used to make learned dynamical models reliable for prediction and control. Revay et al. (2024) introduced Recurrent Equilibrium Networks (REN), a class of nonlinear recurrent models with built-in stability guarantees and contraction properties. REN are suitable for input-output system identification because they can represent history-dependent stable operators, and we use them as the stable operator class for the partially observable Meta-ICI setting. Kojima & Okamoto (2022) proposed learning deep input-output stable dynamics by enforcing a Hamilton-Jacobi inequality, directly targeting input-output stability of neural dynamical systems. In our work, stability is a requirement for compatibility with the ICI framework. While existing recurrent stable models (such as REN) offer stability guarantees and support unconstrained optimization, their inherent reliance on contiguous data sequences to infer hidden states makes them inapplicable when only fragmented data points are available for few-shot target adaptation. For the fully observable setting, we overcome this by designing a SK operator. It operates purely on independent discrete state transitions, naturally accommodating fragmented adaptation data, while intrinsically maintaining the spectral-radius constraint under standard unconstrained gradient descent.

**Notation:** For a sequence $x = \{x_t\}_{t\geq 0}$ with $x_t \in \mathbb{R}^{d_x}$, we write $x \in \ell_p^{d_x}$ if $\|x\|_{\ell_p} = \left(\sum_{t=0}^{\infty} \|x_t\|^p\right)^{1/p} < \infty, 1 \leq p < \infty$, and $x \in \ell_\infty^{d_x}$ if $\|x\|_{\ell_\infty} = \sup_{t\geq 0} |x_t| < \infty$. When the dimension is clear from context, we simply write $\ell_p$. An input-output operator $\Upsilon : \ell^{d_x} \to \ell^{d_y}$ maps an input sequence to an output sequence. It is causal if

the output at time $t$ depends only on the input history up to time $t$, and strictly causal if the output at time $t$ depends only on the input history before time $t$. A causal operator $\Upsilon$ is $\mathcal{L}_p$-stable if $x \in \ell_p^{d_x} \Longrightarrow \Upsilon(x) \in \ell_p^{d_y}$. It is incrementally $\mathcal{L}_p$-stable if there exists $\gamma \in [0, \infty)$ such that $\|\Upsilon(x) - \Upsilon(y)\|_{\ell_p} \leq \gamma \|x - y\|_{\ell_p}, \forall x, y \in \ell_p^{d_x}$. The sets of causal and strictly causal $\mathcal{L}_p$-stable operators are denoted by $\mathcal{L}_p^C$ and $\mathcal{L}_p^{SC}$, respectively.

## 3 Problem Formulation

We consider a family of unknown discrete-time nonlinear plants observed under feedback control. For each task $\mathcal{T}_i$, the plant is represented as a strictly causal input-output operator $G_i$. For a finite horizon, the measured output is written as

$$y_t^{(i)} = G_{i,t}(u_{0:t-1}^{(i)}) + v_t^{(i)}, \qquad t = 0, \ldots, T,$$

where $u_t^{(i)} \in \mathbb{R}^{n_u}$ is the plant input, $y_t^{(i)} \in \mathbb{R}^{n_y}$ is the measured output, and $v_t^{(i)}$ denotes unmeasured disturbances and measurement noise. Equivalently, using sequence notation,

$$y^{(i)} = G_i(u^{(i)}) + v^{(i)}. \tag{1}$$

The plant operates in closed loop with a known causal output-feedback controller $K_i$ and an external reference signal $r_t^{(i)}$:

$$u^{(i)} = r^{(i)} + K_i(y^{(i)}). \tag{2}$$

Thus, the collected data consist of closed-loop trajectories

$$\mathcal{D}_i = \left\{ \left( r_{0:T-1}^{(i,j)}, u_{0:T-1}^{(i,j)}, y_{0:T}^{(i,j)} \right) \right\}_{j=1}^{N_i}.$$

We assume that the closed-loop interconnection is well posed and $\mathcal{L}_p$-stable, i.e., the mapping $(r^{(i)}, v^{(i)}) \mapsto (u^{(i)}, y^{(i)})$ is an $\mathcal{L}_p$-stable operator.

The objective is to identify an open-loop dynamics model $\hat{G}_\star$ for a new target plant $G_\star$ using only limited and possibly fragmented target closed-loop data. This differs from standard open-loop neural system identification methods (Chakrabarty et al., 2023; 2025; Rufolo et al., 2025; Forgione et al., 2025), because the input $u_t$ is not chosen independently of the plant output. Since $u_t$ is generated through feedback from noisy measurements, the regressors used for prediction can be statistically coupled with disturbances and measurement noise. Consequently, directly fitting a neural model on closed-loop trajectories may produce biased models unless additional assumptions, excitation, or identification structure are used (Forssell & Ljung, 1999; Ljung, 1998; Boroujeni et al., 2025). In the few-shot setting, this difficulty is further compounded because the target data may provide only limited coverage of the state-input region needed for counterfactual open-loop rollouts.

We assume access to a collection of related source tasks $\mathcal{T}_i \overset{\text{i.i.d.}}{\sim} p(\mathcal{T}), i = 1, \ldots, M$, where each task corresponds to a closed-loop system with compatible input-output dimensions and known controller $K_i$. The tasks share a common structural class, such as related physical dynamics or common modeling assumptions, but may differ in their system parameters, nonlinearities, or operating conditions. Each source task provides a relatively richer closed-loop dataset $\mathcal{D}_i$. In contrast, the target task $\mathcal{T}_\star$ provides only a small adaptation dataset $\mathcal{D}_\star^{\text{adapt}}$, which may consist of a few short closed-loop trajectories or, in the fully observable case, scattered one-step transitions rather than continuous trajectories.

Therefore, the few-shot closed-loop neural system identification problem is to use the source datasets $\{\mathcal{D}_i\}_{i=1}^M$ to learn a transferable model prior that can be rapidly adapted to the target system $\theta'_\star = \mathcal{A}_\alpha(\theta, \mathcal{D}_\star^{\text{adapt}})$, where $\theta$ denotes the shared initialization and $\mathcal{A}_\alpha$ denotes a small number of adaptation steps with learning rate $\alpha$. The adapted parameters $\theta'_\star$ are then used to construct an open-loop model $\hat{G}_{\theta'_\star}$ for the target plant.

At the meta-training stage, each source dataset is split into a support set and a query set. The support set simulates the limited target data available during adaptation, while the query set evaluates the post-adaptation model. The loss used for adaptation need not be identical to the loss used for meta-evaluation.

In particular, the support loss determines how the model is adapted from limited data, whereas the query loss determines which adapted models are preferred by the meta-objective.

Following the gradient-based meta-learning formulation of MAML (Finn et al., 2017), given an initialization $\theta$, the task-specific adapted parameter is obtained by a small number of gradient steps on a support loss. For one-step adaptation, this gives

$$\theta_i' = \mathcal{A}_\alpha(\theta, \mathcal{D}_i^{\text{sup}}) = \theta - \alpha \nabla_\theta \mathcal{L}_i^{\text{sup}}(\theta, \mathcal{D}_i^{\text{sup}}), \tag{3}$$

with the extension to multiple adaptation steps being straightforward. The meta-objective then evaluates the adapted parameter on a query loss:

$$\min_\theta \ \mathbb{E}_{\mathcal{T}_i \sim p(\mathcal{T})} \left[ \mathcal{L}_i^{\text{qry}} \left( \theta_i', \mathcal{D}_i^{\text{qry}} \right) \right]. \tag{4}$$

Different choices of $\mathcal{L}_i^{\text{sup}}$ and $\mathcal{L}_i^{\text{qry}}$ lead to different instantiations of the proposed framework. For general partially observable systems, adaptation must usually be performed on contiguous trajectories, since the model needs temporal context to infer unmeasured internal states. In this case, both the support and query losses are naturally sequence-based. For fully observable systems, however, each transition already contains the complete state information needed for one-step prediction. This makes it possible to use a step-wise support loss on scattered transitions during adaptation, while still using a sequence-wise query loss to select initializations that produce accurate long-horizon rollouts after adaptation.

## 4 Proposed Approach

This section presents the meta-learning framework for few-shot closed-loop neural system identification. We first introduce Meta-ICI, which combines the ICI reparameterization with gradient-based meta-learning. The ICI structure provides a closed-loop identification parameterization through a stable internal operator, while meta-learning provides an initialization that can be adapted from limited target data. We then introduce Fast Meta-ICI for the fully observable setting, where the availability of the full state allows target adaptation to use scattered one-step transitions instead of contiguous trajectories.

### 4.1 Meta-ICI Framework

For each task $\mathcal{T}_i$, the unknown plant $G_i$ operates in closed loop with a known causal controller $K_i$. Our goal is to use a neural network to identify the open-loop dynamics of target system $G_\star$ from closed-loop data while retaining the prior knowledge that $K_\star$ stabilizes the true plant.

We build on the ICI parameterization, which introduces a strictly causal stable internal operator $S_i \in \mathcal{L}_p^{SC}$, satisfies

$$\hat{y}^\circ = S_i\big(\hat{u} - K_i(\hat{y}^\circ)\big), \tag{5}$$

where $\hat{u}$ is a candidate open-loop input and $\hat{y}^\circ$ is the nominal model output, and defines the corresponding plant model $\hat{G}_i$ through the interconnection

$$\hat{y}^\circ = \hat{G}_i(\hat{u}). \tag{6}$$

The relevance of equation 5 and equation 6 follows the theorem (see Boroujeni et al., 2025, Theorem 1):

If $K_i$ is incrementally $\mathcal{L}_p$-stable, then any choice of $S_i \in \mathcal{L}_p^{SC}$ constructed by equation 5 defines a model $\hat{G}_i$ satisfying equation 6, whose closed-loop interconnection with $K_i$ is $\mathcal{L}_p$-stable. Conversely, if a strictly causal plant $G_i$ is stabilized by $K_i$, then there exists an operator $S_i \in \mathcal{L}_p^{SC}$ such that $G_i = \hat{G}_i$, where $\hat{G}_i$ satisfies equation 6. Thus, learning the plant within the class of systems stabilized by $K_i$ can be reduced to learning the internal operator $S_i$.

It remains to specify how $S_i$ is learned from closed-loop data. Following the indirect training strategy (Boroujeni et al., 2025), we exploit the closed-loop relation in equations 1, 2 and 5. For the closed-loop

model, the noisy output can be written as

$$\hat{y} = S_i\big(\hat{u} - K_i(\hat{y} - v)\big) + v = S_i\big(r + K_i(\hat{y}) - K_i(\hat{y} - v)\big) + v.$$

If $S_i$ and $K_i$ are locally approximated by their linearizations, then $\hat{y} \approx S_i(r) + S_{i,L}(K_{i,L}(v)) + v$, where $S_{i,L}$ and $K_{i,L}$ denote the corresponding local linearizations. This linearized approximation holds well at high output signal-to-noise ratio (SNR) and high excitation SNR. This formulation separates $r$ and $v$ such that the identification of $S_i$ with closed-loop data becomes a standard open-loop identification, which motivates the indirect learning objective $r^{(i)} \mapsto y^{(i)}$ for estimating $S_i$.

We parameterize the internal operator by a stable neural operator $S_\theta$. For a trajectory $\tau^{(i,j)} = \left(r^{(i,j)}_{0:T-1}, y^{(i,j)}_{0:T}\right)$, the predicted output is $\hat{y}^{(i,j)}_{0:T} = S_\theta\left(r^{(i,j)}_{0:T-1}\right)$. The sequence prediction loss for task $\mathcal{T}_i$ on a dataset $\mathcal{D}$ is defined as

$$\mathcal{L}_i^{\text{seq}}(\theta, \mathcal{D}) = \frac{1}{|\mathcal{D}|} \sum_{\tau^{(i,j)} \in \mathcal{D}} \sum_{t=0}^{T} \left\| y_t^{(i,j)} - \hat{y}_t^{(i,j)} \right\|^2.$$

Meta-ICI applies the meta-learning formulation introduced in Section 3 to the ICI internal operator. For general partially observable systems, the model must use temporal context to infer hidden internal states. Therefore, both adaptation and meta-evaluation are performed on contiguous trajectories, which means that $\mathcal{L}_i^{\text{sup}} = \mathcal{L}_i^{\text{seq}}, \mathcal{L}_i^{\text{qry}} = \mathcal{L}_i^{\text{seq}}$.

After meta-training by equation 3 and equation 4, we get the learned initialization $\theta^\star$, which is adapted to a new target task using the limited target adaptation dataset:

$$\theta'_\star = \mathcal{A}_\alpha(\theta^\star, \mathcal{D}_\star^{\text{adapt}}).$$

The final target open-loop model is then constructed through the ICI relation

$$\hat{G}_{\theta'_\star}(\bar{u}) = \bar{y}, \qquad \bar{y} = S_{\theta'_\star}\big(\bar{u} - K_\star(\bar{y})\big), \tag{7}$$

where $\bar{u}$ denotes the input applied to the reconstructed open-loop plant.

**Remark 1.** The ICI representation is applied task-wise. Each task $\mathcal{T}_i$ may have its own known controller $K_i$, and the corresponding internal operator $S_i$ is defined with respect to this controller. Meta-ICI therefore does not require all tasks to share the same controller, nor does it meta-learn the controller itself. Instead, it meta-learns an initialization for the family of ICI-induced internal operators $\{S_i\}$. Successful transfer is assumed at the level of these induced operators, rather than at the level of the plant or controller alone. At target time, the adapted operator $S_{\theta'_\star}$ is combined with the target controller $K_\star$ through the ICI relation to construct the open-loop model.

This formulation is agnostic to the specific stable neural operator used to parameterize $S_\theta$. For partially observable systems, recurrent stable operators such as REN (Revay et al., 2024) are natural choices because they can represent history-dependent input-output maps. However, when the full state is observable, the Markov structure allows a more efficient instantiation in which adaptation is performed using scattered one-step transitions, while meta-training still evaluates long-horizon rollout behavior. The resulting fully observable instantiation is Fast Meta-ICI.

### 4.2 Fast Meta-ICI for Fully Observable Systems

We now specialize Meta-ICI to the fully observable setting. Throughout this subsection, we assume that the measured output is the full state $y_t^{(i)} = x_t^{(i)} \in \mathbb{R}^{n_x}$. In the general input-output setting, the internal operator $S_\theta$ is learned from reference-output trajectories and must use temporal history to represent hidden dynamics. When the full state is observable, this history dependence is no longer necessary. The ICI internal operator $S_i$ can instead be implemented as a Markovian one-step transition model

$$x_{t+1}^{(i)} = f_\theta\left(x_t^{(i)}, r_t^{(i)}\right),$$

where $f_\theta$ is the neural network implementation of $S_i$, $r_t^{(i)}$ is the same reference signal used as the input in Section 4.1.

#### 4.2.1 Schur-Koopman Operator

To instantiate the fully observable internal operator $f_\theta$, we need a neural transition model compatible with the $\mathcal{L}_p^{SC}$ requirement of ICI. A direct way to obtain stability is to enforce contraction of the map, for instance by applying spectral normalization to the neural network (Miyato et al., 2018). Although this strategy is general, it controls stability by requiring every one-step update to contract in a prescribed norm. This requirement can be stronger than necessary for stable dynamics with oscillations, transient amplification, or light damping, where the trajectory may exhibit local growth before eventually decaying (Trefethen & Embree, 2005).

For linear systems, stability is governed by the spectral radius of the state-transition matrix rather than by its spectral norm. A matrix with spectral radius smaller than one may still have spectral norm larger than one, allowing transient amplification while remaining asymptotically stable (Hespanha, 2018). The Koopman-inspired structure lets us exploit this distinction by lifting the nonlinear state into a latent space, evolving it with a linear operator, and decoding it back to the state space (Lusch et al., 2018).

The Koopman-inspired internal operator consists of an encoder $\phi_\theta : \mathbb{R}^{n_x} \to \mathbb{R}^{n_z}$, a decoder $\psi_\theta : \mathbb{R}^{n_z} \to \mathbb{R}^{n_x}$, a latent transition matrix $A_\theta \in \mathbb{R}^{n_z \times n_z}$, and a state-dependent input map $g_\theta : \mathbb{R}^{n_x} \to \mathbb{R}^{n_x \times n_u}$. The transition model is

$$x_{t+1} = f_\theta(x_t, r_t) = \psi_\theta(A_\theta \phi_\theta(x_t)) + g_\theta(x_t) r_t. \tag{8}$$

The spectral-radius constraint on $A_\theta$ is not sufficient to guarantee $\mathcal{L}_p$ stability of the nonlinear operator, because the encoder-decoder composition may distort the latent dynamics. The following theorem states the stability condition required by the system 8.

**Theorem 1.** *Consider the zero-initial-state system induced by equation 8. Assume that: (i) $\phi_\theta$ and $\psi_\theta$ are Lipschitz continuous with Lipschitz constant $L_\psi$ and $L_\phi$ respectively, and satisfy $\phi_\theta(0) = 0$ and $\psi_\theta(0) = 0$; (ii) $g_\theta$ is bounded on the compact operating domain, i.e., there exists $M > 0$ such that $\|g_\theta(x_t)\|_2 \le M$ for all admissible $x_t$; and (iii) the latent autonomous map*

$$F_\theta(z_t) = \phi_\theta(\psi_\theta(A_\theta z_t)) \tag{9}$$

*is a strict contraction in some norm $\|\cdot\|_P$, namely there exists $\lambda \in (0,1)$ such that $\|F_\theta(z_t)\|_P \le \lambda \|z_t\|_P, \forall z_t$. Then the operator mapping the input sequence $r \in \ell_p$ to the state sequence $x \in \ell_p$ is $\mathcal{L}_p$-stable for all $p \in [1, \infty]$. That is, there exists a constant $C > 0$ such that $\|x\|_{\ell_p} \le C\|r\|_{\ell_p}$.*

The proof is provided in Appendix B.

Theorem 1 shows that the key remaining requirement is the contraction of the nonlinear latent autonomous map 9. We now relate this condition to two implementable design choices.

Let $z_{t+1}^A = A_\theta z_t$ and $\Delta_\theta(z_{t+1}^A) = \phi_\theta(\psi_\theta(z_{t+1}^A)) - z_{t+1}^A$. Then $F_\theta(z_t) = A_\theta z_t + \Delta_\theta(A_\theta z_t)$.

Suppose that the latent transition is Schur stable, i.e., $\rho(A_\theta) < 1$. By the spectral-radius lemma (Horn & Johnson, 2012), there exists an induced norm $\|\cdot\|_P$ and a constant $\rho_P \in (0,1)$ such that $\|A_\theta z_t\|_P \le \rho_P \|z_t\|_P$.

In addition, if the encoder-decoder residual $\Delta_\theta(\cdot)$ is sufficiently small, i.e., $\|\Delta_\theta(A_\theta z_t)\|_P \le \delta \|A_\theta z_t\|_P, \delta \ge 0$, then applying the triangle inequality gives

$$\|F_\theta(z_t)\|_P \le \|A_\theta z_t\|_P + \|\Delta_\theta(A_\theta z_t)\|_P \le (1+\delta)\|A_\theta z_t\|_P \le (1+\delta)\rho_P \|z_t\|_P.$$

Therefore, whenever $\delta$ is small enough such that $\lambda = (1+\delta)\rho_P < 1$, the nonlinear latent autonomous map 9 satisfies the contraction condition required in Theorem 1.

Therefore, we add

$$\mathcal{L}_{\text{rec}}(\theta, \mathcal{D}) = \frac{1}{|\mathcal{Z}_{\mathcal{D}}^A|} \sum_{\tilde{z} \in \mathcal{Z}_{\mathcal{D}}^A} \|\tilde{z} - \phi_\theta(\psi_\theta(\tilde{z}))\|_2^2, \qquad \mathcal{Z}_{\mathcal{D}}^A = \{A_\theta \phi_\theta(x_t) : (x_t, \cdot, \cdot) \in \mathcal{D}\}. \tag{10}$$

Since the latent space is finite-dimensional, norm equivalence implies that controlling the Euclidean reconstruction residual also controls the same residual in $\|\cdot\|_P$ up to constant factors (Horn & Johnson, 2012).

Thus, the reconstruction loss empirically targets the residual term required by the sufficient contraction condition.

It remains to enforce the spectral-radius condition $\rho(A_\theta) < 1$. To this end, we parameterize $A_\theta$ through a real Schur form

$$A_\theta = Q_\theta T_\theta Q_\theta^\top, \qquad T_\theta = D_\theta + U_\theta.$$

Here, $Q_\theta$ is an orthogonal matrix and $T_\theta$ is a real quasi-upper triangular matrix. The block diagonal part $D_\theta$ contains $2 \times 2$ rotation-scaling blocks

$$R_k = \rho_k \begin{bmatrix} \cos\omega_k & -\sin\omega_k \\ \sin\omega_k & \cos\omega_k \end{bmatrix}, \qquad \rho_k = \bar{\rho}\,\sigma(a_k), \qquad 0 < \bar{\rho} < 1, \tag{11}$$

with a possible $1 \times 1$ block when $n_z$ is odd, where $\sigma$ is the sigmoid function. The matrix $U_\theta$ contains learnable entries only in the strictly block upper-triangular part associated with this Schur block partition. Consequently, $T_\theta$ remains block upper triangular, and its eigenvalues are exactly the eigenvalues of the diagonal blocks in $D_\theta$. Since each block has eigenvalue magnitude smaller than $\bar{\rho}$, the construction guarantees $\rho(A_\theta) = \rho(T_\theta) < \bar{\rho} < 1$.

This parameterization is useful not only as a stability-enforcing construction, but also as an optimization device. The spectral-radius constraint is satisfied by construction for any values of the unconstrained trainable parameters that define equation 11. Therefore, the constrained optimization problem over stable latent transition matrices is transformed into an unconstrained optimization problem over the Schur parameters. This avoids projection steps, eigenvalue clipping, or custom constrained solvers, and allows the SK operator to be trained with standard neural network optimizers such as SGD and Adam. Importantly, this construction enforces the latent spectral-radius condition throughout training, while the reconstruction loss in equation 10 encourages the encoder-decoder composition to preserve the contraction condition required by Theorem 1.

#### 4.2.2 Hybrid Step-wise/Sequence-wise Meta-Objective

The fully observable setting allows the support and query losses to use different data formats. Therefore, the support set may consist of scattered one-step transitions, $\mathcal{D}_i^{\text{sup}} = \left\{ (x_t^{(i,j)}, r_t^{(i,j)}, x_{t+1}^{(i,j)}) \right\}$, while the query set consists of contiguous rollout segments, $\mathcal{D}_i^{\text{qry}} = \left\{ (x_0^{(i,j)}, r_{0:H-1}^{(i,j)}, x_{1:H}^{(i,j)}) \right\}$.

Consequently, the support loss is a one-step-wise transition loss:

$$\mathcal{L}_i^{\text{step}}(\theta, \mathcal{D}_i^{\text{sup}}) = \frac{1}{|\mathcal{D}_i^{\text{sup}}|} \sum_{(x_t, r_t, x_{t+1}) \in \mathcal{D}_i^{\text{sup}}} \|x_{t+1} - f_\theta(x_t, r_t)\|^2 + \lambda_{\text{rec}} \mathcal{L}_{\text{rec}}(\theta, \mathcal{D}_i^{\text{sup}}).$$

The adapted parameter, $\theta_i' = \mathcal{A}_\alpha^{\text{step}}(\theta, \mathcal{D}_i^{\text{sup}})$, for task $\mathcal{T}_i$ is obtained by applying one or more gradient steps on this support loss.

The query loss evaluates the adapted model through multi-step rollout. That is, given an initial state $x_0$ and a reference sequence $r_{0:H-1}$, the predicted rollout is generated by

$$\hat{x}_0 = x_0, \qquad \hat{x}_{t+1} = f_{\theta_i'}(\hat{x}_t, r_t), \qquad t = 0, \ldots, H-1.$$

The sequence-wise query loss is

$$\mathcal{L}_i^{\text{roll}}(\theta_i', \mathcal{D}_i^{\text{qry}}) = \frac{1}{|\mathcal{D}_i^{\text{qry}}|} \sum_{(x_0, r_{0:H-1}, x_{1:H}) \in \mathcal{D}_i^{\text{qry}}} \sum_{t=0}^{H-1} \|x_{t+1} - \hat{x}_{t+1}\|^2 + \lambda_{\text{rec}} \mathcal{L}_{\text{rec}}(\theta, \mathcal{D}_i^{\text{qry}}).$$

Fast Meta-ICI uses the step-wise loss for adaptation and the rollout loss for meta-evaluation, i.e., $\mathcal{L}_i^{\text{sup}} = \mathcal{L}_i^{\text{step}}, \mathcal{L}_i^{\text{qry}} = \mathcal{L}_i^{\text{roll}}$.

After meta-training, the learned initialization $\theta^\star$ is adapted to the target system using the fragmented target adaptation set $\mathcal{D}_\star^{\text{adapt}} = \{(x_t, r_t, x_{t+1})\}$, yielding $\theta_\star' = \mathcal{A}_\alpha^{\text{step}}\left(\theta^\star, \mathcal{D}_\star^{\text{adapt}}\right)$. The adapted model is then evaluated or deployed through the ICI open-loop reconstruction in equation 7.

# 5 Experiments

We design our empirical evaluation to validate the properties of the proposed frameworks. Specifically, our experiments aim to answer the following questions:

- **Q1 (Data Efficiency in Partial Observability):** To what extent does the Meta-ICI framework using recurrent structures improve data efficiency when adapting to an unseen controlled system under partial observability?
- **Q2 (Fragmented Adaptation under Shifted Inputs):** Under fully observable conditions, can Fast Meta-ICI recover full-data-level long-horizon predictive accuracy from fragmented target data, even when evaluated on input families not seen during training?

Throughout the experiments, we compare the proposed few-shot adaptation methods against full-data references trained with abundant target-system data under the same model class and evaluation protocol. They serve as strong empirical baselines indicating the performance attainable by the same architecture when substantially richer target data are available.

Detailed experimental configurations are deferred to Appendices A.1 and A.2.

## 5.1 Efficiency under Partial Observability

To answer **Q1**, we evaluate the Meta-ICI framework on a family of partially observable Liénard systems. The nonlinear damping parameter defines the system family, and we select one unseen target system for adaptation. Only the first state is measured, while the second state remains hidden. Detailed dynamics, controller, and signal-generation settings are provided in Appendix A.1.1.

For the stable operator $\boldsymbol{S}_\theta$, we employ a Contractive Recurrent Equilibrium Network (C-REN). As a recurrent architecture, it is naturally suited for partially observable settings by maintaining hidden states to infer unmeasured dynamics, while its parameterization intrinsically guarantees the strictly causal and stable condition ($\mathcal{L}_p^{SC}$) required by the Meta-ICI framework.

**Evaluation Protocol and Baselines.** We assess the predictive performance using the FIT score, defined as $\text{FIT} = 100 \times \left(1 - \frac{\|\hat{y}-y\|_2}{\|y-\bar{y}\|_2}\right)$, where $y$ is the true trajectory, $\bar{y}$ is its mean, and $\hat{y}$ is the predicted trajectory. A FIT of 100% indicates perfect prediction. For a rigorous comparison, all evaluated models are tested under identical initial conditions and excitation signals. All reported FIT values are the mean $\pm$ standard deviation computed over 5 random seeds. We compare our proposed **Meta-ICI** against two baselines: (1) **Full-Data ICI Reference**, trained on 100 target-system trajectories under the same C-REN architecture, and (2) **Scratch ICI**, a C-REN initialized with random weights and fine-tuned exclusively on the limited target data.

As summarized in Table 1, the results demonstrate that Meta-ICI consistently and significantly outperforms Scratch ICI across all regimes. Meta-ICI rapidly approaches the Full-Data ICI Reference (75.16%) even in extreme few-shot scenarios. With merely 3 trajectories, the performance reaches 64.13%. Furthermore, a larger data size significantly accelerates the initial performance gain: 10 trajectories achieve 34.73% compared to $-4.69\%$ for 1 trajectory at step 3, showing that richer data provides a better gradient direction.

## 5.2 Robustness to Fragmented Data and Long-Horizon Stability

To answer **Q2**, we shift our focus to fully observable dynamics and evaluate the proposed Fast Meta-ICI method on a nonlinear pendulum benchmark. The central question is whether Fast Meta-ICI can identify an accurate long-horizon dynamics model from fragmented few-shot target data, while approaching full-data reference performance even under test inputs not seen during training. The target adaptation data consist only of scattered single-step transitions, whereas evaluation is performed through continuous 200-step open-loop rollouts. This deliberately separates the data format available for adaptation from the long-horizon predictive behavior required at test time.

Table 1: Predictive FIT [%] results under partial observability. Meta-ICI achieves superior data efficiency. It exceeds 64% FIT with as few as 3 target trajectories, approaching the Full-Data ICI Reference trained on 100 target trajectories. Larger data sizes lead to faster early-stage improvement, and the consistent upward trend across adaptation steps highlights rapid convergence. In contrast, Scratch ICI remains ineffective under identical conditions. All reported values are the mean ± standard deviation across 5 random seeds.

| **Method** | **Data Size** | **Adaptation Steps** | | | | |
|---|---|---|---|---|---|---|
| | | **0** | **1** | **3** | **5** | **10** |
| **Full-Data ICI Reference** | 100 Trajs | | | $75.16 \pm 8.47$ | | |
| **Meta-ICI** (Ours) | 1 Traj | $-73.26 \pm 20.52$ | $-47.62 \pm 17.47$ | $-4.69 \pm 11.55$ | $26.95 \pm 7.56$ | $58.79 \pm 8.91$ |
| | 3 Trajs | | $-40.30 \pm 17.13$ | $14.12 \pm 9.98$ | $47.92 \pm 8.29$ | $64.13 \pm 12.07$ |
| | 5 Trajs | – | $-31.73 \pm 15.85$ | $33.47 \pm 7.94$ | $57.83 \pm 11.03$ | $64.15 \pm 12.63$ |
| | 8 Trajs | | $-34.04 \pm 16.31$ | $30.46 \pm 8.19$ | $57.48 \pm 10.61$ | $64.37 \pm 12.57$ |
| | 10 Trajs | | $-32.05 \pm 15.71$ | $34.73 \pm 7.84$ | $58.36 \pm 11.08$ | $64.30 \pm 12.38$ |
| **Scratch ICI** | 1 Traj | $-97.78 \pm 37.54$ | $-76.36 \pm 35.07$ | $-52.10 \pm 32.13$ | $-39.82 \pm 30.43$ | $-28.38 \pm 28.38$ |
| | 3 Trajs | | $-74.95 \pm 34.93$ | $-49.86 \pm 31.91$ | $-37.58 \pm 30.16$ | $-26.69 \pm 28.10$ |
| | 5 Trajs | – | $-73.51 \pm 34.76$ | $-47.30 \pm 31.56$ | $-34.81 \pm 29.69$ | $-24.41 \pm 27.51$ |
| | 8 Trajs | | $-74.17 \pm 34.83$ | $-47.94 \pm 31.63$ | $-35.12 \pm 29.73$ | $-24.25 \pm 27.45$ |
| | 10 Trajs | | $-73.21 \pm 34.69$ | $-46.55 \pm 31.37$ | $-33.91 \pm 29.42$ | $-23.69 \pm 27.16$ |

**Protocol.** Training data are collected from closed-loop trajectories driven by randomized bounded multi-sine references, while testing uses open-loop zero-input responses and step responses. The zero-input tests measure recovery of autonomous dynamics, while the step responses evaluate forced dynamics under inputs not used during training. Fast Meta-ICI adapts from randomly sampled single-step target transitions. Detailed system parameters and data-generation settings are provided in Appendix A.2.1. Validation grids and optimization hyperparameters are provided in Appendices A.2.2 and A.2.3.

**Compared models. Full-Data SK-ICI Reference** is a SK model trained with abundant continuous target-system trajectories under the same architecture and test protocol. **Fast Meta-ICI** uses the SK architecture with the Hybrid MAML initialization, then adapts on the fragmented target data. The comparison focuses on whether few-shot adaptation can approach this empirical full-data reference under qualitatively shifted test inputs. For completeness, we also ran a **Scratch SK** baseline with the same SK architecture and fragmented target adaptation data but random initialization. This baseline uses no meta-learned initialization and no learned inner-loop learning rates.

**Metric and model selection.** Because zero-input and small-amplitude responses can have low signal energy, FIT scores may become unstable under this protocol. We therefore report NRMSE separately for $\theta$ and $\omega$. Each rollout is divided into four consecutive, non-overlapping step-index segments $Q_1 = [0, 50)$, $Q_2 = [50, 100)$, $Q_3 = [100, 150)$, and $Q_4 = [150, 200)$. $Q_1$ captures short-horizon accuracy, while $Q_4$ captures late-horizon error accumulation. For state coordinate $j \in \{\theta, \omega\}$ and segment $Q_q$, we compute

$$\mathrm{NRMSE}_j^{(q)} = \frac{\sqrt{\frac{1}{|I_q|}\sum_{t\in I_q}(x_{t,j} - \hat{x}_{t,j})^2}}{\sqrt{\frac{1}{|I_q|}\sum_{t\in I_q} x_{t,j}^2} + \epsilon},$$

where $I_q$ is the time-index set of segment $Q_q$. All checkpoints and adaptation steps are selected using held-out zero-input and step-response validation rollouts. The final test set is used only for reporting. Table entries are reported as mean ± standard deviation across repeated runs. Additional validation and reporting details are specified in Appendix A.2.2.

**Quantitative results.** Tables 2 and 3 report segmented NRMSE for $\theta$ and $\omega$, respectively. After validation selection, Scratch SK diverged in rollout evaluation across seeds. We therefore exclude it from the main quantitative tables. This failure indicates that, without meta-learning, the fragmented target data are insufficient to adapt the same SK architecture from a random initialization in this task. The results show that Fast Meta-ICI remains non-divergent over the full rollout horizon and achieves performance comparable to the Full-Data SK-ICI Reference under step-response tests, while a visible gap remains in the late zero-input segments.

Table 2: Segmented NRMSE for the angle state $\theta$ over 200-step rollouts. Zero-input and step-response tests are reported separately. Lower is better.

| Method | Zero-input tests | | | | Step-response tests | | | |
|---|---|---|---|---|---|---|---|---|
| | $Q_1$ | $Q_2$ | $Q_3$ | $Q_4$ | $Q_1$ | $Q_2$ | $Q_3$ | $Q_4$ |
| Full-Data SK-ICI Reference | $0.1211 \pm 0.0241$ | $0.2262 \pm 0.0277$ | $0.2767 \pm 0.0401$ | $0.3232 \pm 0.0633$ | $0.0876 \pm 0.0311$ | $0.3213 \pm 0.1635$ | $0.1960 \pm 0.0985$ | $0.1609 \pm 0.0915$ |
| **Fast Meta-ICI (Ours)** | $0.1090 \pm 0.0556$ | $0.2845 \pm 0.1210$ | $0.3912 \pm 0.1972$ | $0.3856 \pm 0.1973$ | $0.0922 \pm 0.0182$ | $0.2394 \pm 0.1392$ | $0.2228 \pm 0.01362$ | $0.2243 \pm 0.1930$ |

Table 3: Segmented NRMSE for the angular-velocity state $\omega$ over 200-step rollouts. Zero-input and step-response tests are reported separately. Lower is better.

| Method | Zero-input tests | | | | Step-response tests | | | |
|---|---|---|---|---|---|---|---|---|
| | $Q_1$ | $Q_2$ | $Q_3$ | $Q_4$ | $Q_1$ | $Q_2$ | $Q_3$ | $Q_4$ |
| Full-Data SK-ICI Reference | $0.1418 \pm 0.0357$ | $0.2064 \pm 0.0315$ | $0.2687 \pm 0.0292$ | $0.3204 \pm 0.0503$ | $0.1327 \pm 0.0430$ | $0.4220 \pm 0.1188$ | $0.6337 \pm 0.1461$ | $0.8930 \pm 0.1912$ |
| **Fast Meta-ICI (Ours)** | $0.1335 \pm 0.0605$ | $0.2893 \pm 0.1279$ | $0.3679 \pm 0.1544$ | $0.4591 \pm 0.2419$ | $0.1284 \pm 0.0314$ | $0.3969 \pm 0.0673$ | $0.7468 \pm 0.1765$ | $0.9099 \pm 0.3482$ |

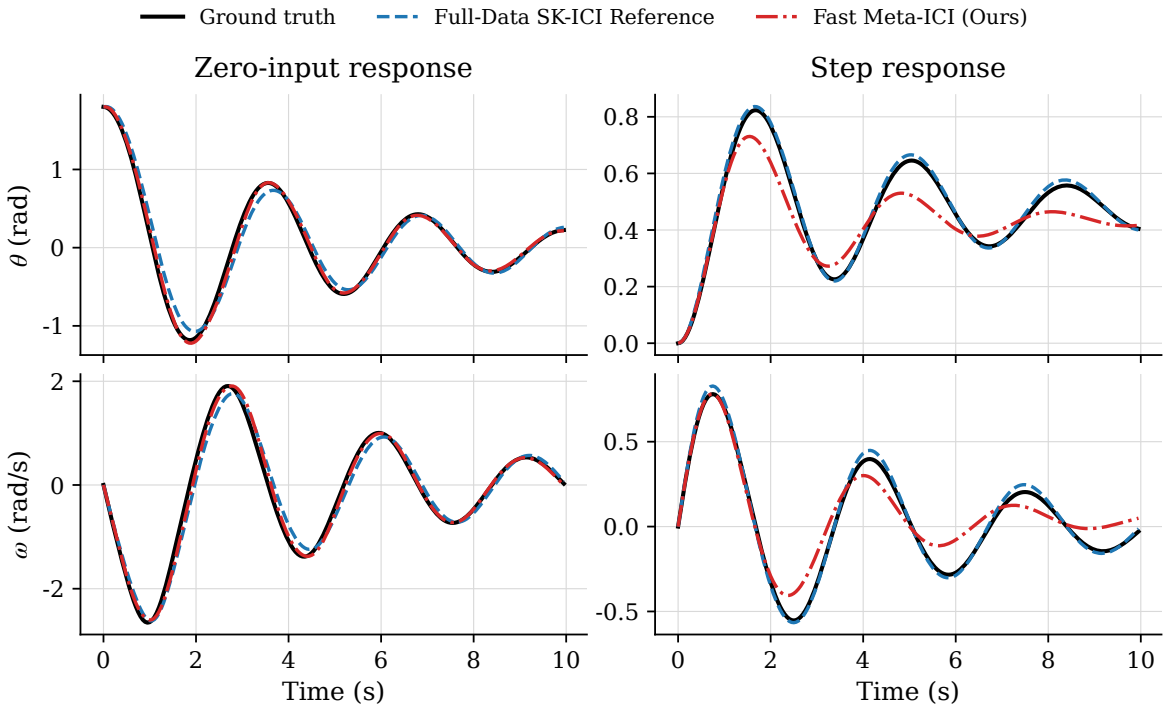


Figure 1: Representative 200-step open-loop rollouts for two selected test scenarios. The zero-input response uses $\theta_0 = 1.8$, $\omega_0 = 0$, and $r_t = 0$. The step response uses $x_0 = 0$ and constant step amplitude $r_t = 1.8$. The upper row shows the angle state $\theta(t)$, and the lower row shows the angular velocity state $\omega(t)$. Fast Meta-ICI is adapted from 200 scattered one-step target transitions and then evaluated on continuous long-horizon rollouts. The zero-input response tests autonomous dynamics recovery, while the step response evaluates forced dynamics under an input family not used during training.

**Representative rollouts.** To complement the segmented NRMSE values, Figure 1 reports two selected test scenarios from the final test set. The zero-input case uses $\theta_0 = 1.8$, $\omega_0 = 0$, and $r_t = 0$, while the step-response case uses $x_0 = 0$ and constant step amplitude $r_t = 1.8$. We use these rollouts as qualitative examples of the adapted model behavior. The main quantitative comparison is given by Tables 2 and 3, which average results over repeated runs and multiple test scenarios, whereas Figure 1 shows one selected case from each input family.

In this representative case, Fast Meta-ICI remains non-divergent over the full 200-step horizon under both input families and captures the dominant oscillatory behavior of the target system. The visible discrepancies reflect both the different state amplitudes and axis scales across panels and the fact that NRMSE is normalized segment-wise by the corresponding signal energy. Overall, the quantitative results show that Fast Meta-ICI approaches the Full-Data SK-ICI Reference on step-response tests, while a late-horizon gap remains on zero-input tests.

## 6 Conclusion

This work shows that closed-loop neural system identification can benefit from meta-learned stable internal operators. Instead of training each target system from scratch, Meta-ICI uses related closed-loop systems to provide an adaptive prior for the internal operator, making few-shot adaptation feasible under feedback-controlled data. A central outcome is that full-state observability makes the few-shot setting substantially easier to exploit. Fast Meta-ICI uses this structure so that adaptation can be performed with scattered one-step transitions, while the learned initialization is still selected for long-horizon rollout behavior. This is the main practical advantage of the method, since fragmented target data are common when long continuous target experiments are unavailable. The experiments support these conclusions in two complementary regimes. The Liénard benchmark shows that meta-learned internal operators can provide a useful prior when hidden dynamics require recurrent stable models. The pendulum benchmark shows that, when the state is fully observable, fragmented one-step target data can still guide a model toward reliable long-horizon counterfactual behavior. Future work should test this rollout-oriented prior on higher-dimensional controlled systems and examine its robustness to weaker task relatedness.

## References

Gerben I. Beintema, Maarten Schoukens, and Roland Tóth. Continuous-time identification of dynamic state-space models by deep subspace encoding. In *The Eleventh International Conference on Learning Representations*, 2023. URL https://openreview.net/forum?id=_4n3k3d1ob.

Mahrokh G. Boroujeni, Laura Meroi, Leonardo Massai, Clara L. Galimberti, and Giancarlo Ferrari-Trecate. Neural identification of feedback-stabilized nonlinear systems. In *2025 IEEE 64th Conference on Decision and Control (CDC)*, pp. 4201–4207, 2025. doi: 10.1109/CDC57313.2025.11312335.

Olfa Boubaker. The inverted pendulum benchmark in nonlinear control theory: A survey. *International Journal of Advanced Robotic Systems*, 10(5), January 2013. ISSN 1729-8814. doi: 10.5772/55058. URL http://dx.doi.org/10.5772/55058.

Ankush Chakrabarty, Gordon Wichern, and Christopher R. Laughman. Meta-learning of neural state-space models using data from similar systems. *IFAC-PapersOnLine*, 56(2):1490–1495, 2023. ISSN 2405-8963. doi: https://doi.org/10.1016/j.ifacol.2023.10.1843. URL https://www.sciencedirect.com/science/article/pii/S2405896323022528. 22nd IFAC World Congress.

Ankush Chakrabarty, Gordon Wichern, Vedang M. Deshpande, Abraham P. Vinod, Karl Berntorp, and Christopher R. Laughman. Meta-learning for physically-constrained neural system identification. *Neurocomputing*, 651:130945, 2025. ISSN 0925-2312. doi: https://doi.org/10.1016/j.neucom.2025.130945. URL https://www.sciencedirect.com/science/article/pii/S0925231225016170.

Ricky T. Q. Chen, Yulia Rubanova, Jesse Bettencourt, and David K Duvenaud. Neural ordinary differential equations. In S. Bengio, H. Wallach, H. Larochelle, K. Grauman, N. Cesa-Bianchi,

and R. Garnett (eds.), *Advances in Neural Information Processing Systems*, volume 31. Curran Associates, Inc., 2018. URL https://proceedings.neurips.cc/paper_files/paper/2018/file/69386f6bb1dfed68692a24c8686939b9-Paper.pdf.

Kurtland Chua, Roberto Calandra, Rowan McAllister, and Sergey Levine. Deep reinforcement learning in a handful of trials using probabilistic dynamics models. In S. Bengio, H. Wallach, H. Larochelle, K. Grauman, N. Cesa-Bianchi, and R. Garnett (eds.), *Advances in Neural Information Processing Systems*, volume 31. Curran Associates, Inc., 2018. URL https://proceedings.neurips.cc/paper_files/paper/2018/file/3de568f8597b94bda53149c7d7f5958c-Paper.pdf.

Ignasi Clavera, Anusha Nagabandi, Simin Liu, Ronald S. Fearing, Pieter Abbeel, Sergey Levine, and Chelsea Finn. Learning to adapt in dynamic, real-world environments through meta-reinforcement learning. In *International Conference on Learning Representations*, 2019. URL https://openreview.net/forum?id=HyztsoC5Y7.

Rogier Dinkla, Tom Oomen, Sebastiaan Paul Mulders, and Jan-Willem van Wingerden. Closed-loop data-enabled predictive control and its equivalence with closed-loop subspace predictive control. *Automatica*, 183:112556, 2026. ISSN 0005-1098. doi: https://doi.org/10.1016/j.automatica.2025.112556. URL https://www.sciencedirect.com/science/article/pii/S0005109825004510.

Chelsea Finn, Pieter Abbeel, and Sergey Levine. Model-agnostic meta-learning for fast adaptation of deep networks. In *Proceedings of the 34th International Conference on Machine Learning*, pp. 1126–1135, 2017.

Marco Forgione, Ankush Chakrabarty, Dario Piga, Matteo Rufolo, and Alberto Bemporad. Manifold meta-learning for reduced-complexity neural system identification. *arXiv preprint arXiv:2504.11811*, 2025. URL https://arxiv.org/abs/2504.11811.

Urban Forssell and Lennart Ljung. Closed-loop identification revisited. *Automatica*, 35(7):1215–1241, 1999. ISSN 0005-1098. doi: https://doi.org/10.1016/S0005-1098(99)00022-9. URL https://www.sciencedirect.com/science/article/pii/S0005109899000229.

Lilli Frison and Simon Gölzhäuser. Adaptive neural network based control approach for building energy control under changing environmental conditions. In Alessandro Abate, Mark Cannon, Kostas Margellos, and Antonis Papachristodoulou (eds.), *Proceedings of the 6th Annual Learning for Dynamics and Control Conference*, volume 242 of *Proceedings of Machine Learning Research*, pp. 1741–1752. PMLR, 15–17 Jul 2024. URL https://proceedings.mlr.press/v242/frison24a.html.

João P. Hespanha. *Linear Systems Theory*. Princeton Press, Princeton, New Jersey, February 2018. ISBN13: 9780691179575.

Roger A. Horn and Charles R. Johnson. *Matrix Analysis*. Cambridge University Press, 2 edition, 2012.

Elia Kaufmann, Leonard Bauersfeld, Antonio Loquercio, Matthias Müller, Vladlen Koltun, and Davide Scaramuzza. Champion-level drone racing using deep reinforcement learning. *Nature*, 620(7976):982–987, August 2023. ISSN 1476-4687. doi: 10.1038/s41586-023-06419-4. URL http://dx.doi.org/10.1038/s41586-023-06419-4.

Hassan K Khalil. *Nonlinear systems*. Prentice Hall, Upper Saddle River, N.J., 2002. ISBN 0130673897 9780130673893 0131227408 9780131227408.

Ryosuke Kojima and Yuji Okamoto. Learning deep input-output stable dynamics. In Alice H. Oh, Alekh Agarwal, Danielle Belgrave, and Kyunghyun Cho (eds.), *Advances in Neural Information Processing Systems*, 2022. URL https://openreview.net/forum?id=BTeJpF_BhQ6.

Zhenguo Li, Fengwei Zhou, Fei Chen, and Hang Li. Meta-sgd: Learning to learn quickly for few shot learning. *CoRR*, abs/1707.09835, 2017. URL http://arxiv.org/abs/1707.09835.

Lennart Ljung. *System Identification*, pp. 163–173. Birkhäuser Boston, Boston, MA, 1998. ISBN 978-1-4612-1768-8. doi: 10.1007/978-1-4612-1768-8_11. URL https://doi.org/10.1007/978-1-4612-1768-8_11.

Bethany Lusch, J. Nathan Kutz, and Steven L. Brunton. Deep learning for universal linear embeddings of nonlinear dynamics. *Nature Communications*, 9:4950, 2018. doi: 10.1038/s41467-018-07210-0.

Takeru Miyato, Toshiki Kataoka, Masanori Koyama, and Yuichi Yoshida. Spectral normalization for generative adversarial networks. In *International Conference on Learning Representations*, 2018. URL https://openreview.net/forum?id=B1QRgziT-.

Gianluigi Pillonetto, Aleksandr Aravkin, Daniel Gedon, Lennart Ljung, Antônio H. Ribeiro, and Thomas B. Schön. Deep networks for system identification: A survey. *Automatica*, 171:111907, 2025. ISSN 0005-1098. doi: https://doi.org/10.1016/j.automatica.2024.111907. URL https://www.sciencedirect.com/science/article/pii/S0005109824004011.

Max Revay, Ruigang Wang, and Ian R. Manchester. Recurrent equilibrium networks: Flexible dynamic models with guaranteed stability and robustness. *IEEE Transactions on Automatic Control*, 69(5):2855–2870, 2024. doi: 10.1109/TAC.2023.3294101.

Matteo Rufolo, Dario Piga, and Marco Forgione. Distributionally robust minimization in meta-learning for system identification. *IEEE Control Systems Letters*, 9:1652–1657, 2025. doi: 10.1109/LCSYS.2025.3582634.

Amber Srivastava, Mingzhou Yin, Andrea Iannelli, and Roy S. Smith. A dual system-level parameterization for identification from closed-loop data. In *2023 62nd IEEE Conference on Decision and Control (CDC)*, pp. 4506–4511, 2023. doi: 10.1109/CDC49753.2023.10383298.

Steven H Strogatz. *Nonlinear Dynamics and Chaos: With Applications to Physics, Biology, Chemistry, and Engineering*. Chapman and Hall/CRC, January 2024. ISBN 9780429398490. doi: 10.1201/9780429398490. URL http://dx.doi.org/10.1201/9780429398490.

Lloyd N. Trefethen and Mark Embree. *Spectra and Pseudospectra: The Behavior of Nonnormal Matrices and Operators*. Princeton University Press, January 2005. ISBN 9780691213101. doi: 10.1515/9780691213101. URL http://dx.doi.org/10.1515/9780691213101.

Guangyao Zhou, Sivaramakrishnan Swaminathan, Rajkumar Vasudeva Raju, J Swaroop Guntupalli, Wolfgang Lehrach, Joseph Ortiz, Antoine Dedieu, Miguel Lazaro-Gredilla, and Kevin Patrick Murphy. Diffusion model predictive control. *Transactions on Machine Learning Research*, 2025. ISSN 2835-8856. URL https://openreview.net/forum?id=pvtgffHtJm.

Yun Zhu, Wengang Yan, and Yucai Zhu. Mpc closed-loop identification without excitation. *Journal of Process Control*, 106:122–129, 2021. ISSN 0959-1524. doi: https://doi.org/10.1016/j.jprocont.2021.08.018. URL https://www.sciencedirect.com/science/article/pii/S0959152421001438.

## A Detailed Experimental Settings

This appendix provides the experimental details omitted from the main text. We describe the system dynamics, data-generation procedures, model architectures, optimization settings, and evaluation protocols used in the two experiments. Appendix A.1 gives the details for the partially observable Liénard benchmark, and Appendix A.2 gives the details for the fully observable pendulum benchmark.

### A.1 Liénard System (Experiment 1)

This experiment evaluates Meta-ICI under partial observability. The benchmark uses a controlled Liénard-type nonlinear oscillator, where only the first state is measured and the second state remains hidden. We first describe the system dynamics and closed-loop data collection procedure, then specify the meta-learning data preparation, C-REN architecture, and optimization settings.

### A.1.1 System Dynamics and Data Generation

We use a controlled Liénard-type nonlinear oscillator as the partially observable benchmark (Strogatz, 2024; Khalil, 2002). Liénard systems form a classical family of two-dimensional nonlinear dynamical systems and include well-known nonlinear oscillators such as the van der Pol oscillator. The parameter $c$ controls the nonlinear damping strength, which makes the benchmark suitable for evaluating adaptation across related nonlinear systems.

The continuous-time target family is defined as follows:

$$\begin{aligned}\dot{x}_1 &= x_2,\\ \dot{x}_2 &= -c(1+x_1^2)x_2 - x_1 + u,\end{aligned}$$

where $c \sim \mathcal{U}[0.5, 2.0]$ parameterizes the source-task distribution. The target system uses $c = 1.57$. Only $x_1$ is measured, and $x_2$ is hidden from the model output. The closed-loop input is generated by a proportional controller

$$u_t = r_t - K_p(x_{1,t} + v_t),$$

where $K_p = 0.3 - 0.1c$ for each system and the controller output is clipped to $[-0.5, 0.5]$ before being added to the reference signal.

**Discretization.** The dynamics are numerically simulated using the standard fourth-order Runge-Kutta (RK4) integration method with a fixed time step of $\Delta t = 0.1$ s.

**Excitation signal.** The truncated colored Gaussian noise for the reference signal $r$ is generated by passing standard white noise through a second-order Butterworth low-pass filter with a cutoff frequency of 0.5 Hz. The filtered signal is z-score normalized, scaled to a standard deviation of 2.0, and clipped to the range $[-6.0, 6.0]$.

**Observation noise.** The zero-mean Gaussian observation noise $v$ has a standard deviation of $\sigma = 0.03$ and is truncated at $\pm 3\sigma$.

### A.1.2 Meta-Learning Data Preparation

We uniformly sample 100 source tasks from $c \in [0.5, 2.0]$. For each source task, we run closed-loop simulations to collect 200 independent trajectories, each consisting of 100 time steps. This offline dataset is used only during meta-training, where each task-level update samples disjoint support and query trajectory sets.

### A.1.3 C-REN Architecture

The stable operator $\boldsymbol{S}_\theta$ is parameterized by a C-REN with input dimension 1 and output dimension 1. Let $\xi_t \in \mathbb{R}^{n_\xi}$ denote the C-REN internal state and $w_t \in \mathbb{R}^q$ denote the nonlinear equilibrium variable. The recurrent update has the form

$$\begin{aligned}E\xi_{t+1} &= F\xi_t + B_1 w_t + B_2 r_t,\\ y_t &= C_2\xi_t + D_{21} w_t,\end{aligned}$$

where $w_t$ is computed through a lower-triangular implicit nonlinear block:

$$w_t = \tanh\big(\Lambda^{-1}(C_1\xi_t + D_{11}w_t)\big).$$

In implementation, the components of $w_t$ are solved sequentially because $D_{11}$ is strictly lower triangular. The direct feedthrough terms from $r_t$ to $w_t$ and $y_t$ are omitted, enforcing strict causality with respect to the reference input. Following the C-REN parameterization, the matrices above are derived from a positive definite matrix $H = X^\top X + \epsilon I$ with $\epsilon = 10^{-3}$, which guarantees the contractive condition by construction. We set $n_\xi = 16$ and $q = 16$. The initial C-REN state is initialized from the first measured output using a learned linear map.

#### A.1.4 Optimization and Baselines

**Meta-training.** The MAML inner update uses one gradient-descent step on the full support-set loss with adaptation rate $\alpha = 10^{-1}$, which is a deterministic update of the form $\theta_i' = \theta - \alpha \nabla_\theta \mathcal{L}_{\mathcal{T}_i}(\theta, \mathcal{D}_i^{sup})$. The outer loop uses Adam with meta-learning rate $\beta = 10^{-3}$. Each meta-update uses a task batch size of 8 source tasks. For each source task, the support set contains 5 trajectories and the query set contains 10 trajectories. Meta-training runs for 100 epochs.

**Target adaptation.** After meta-training, Meta-ICI is adapted to the target system using the selected number of target trajectories in Table 1. Each adaptation step is a full-batch gradient descent update on the complete target adaptation set, with learning rate $3 \times 10^{-2}$.

**Baselines.** The **Full-Data ICI Reference** baseline uses the same C-REN architecture and is trained on 100 target-system trajectories with Adam, learning rate $10^{-3}$, batch size 25, and 100 epochs. The **Scratch ICI** baseline is randomly initialized and then adapted on the same target adaptation trajectories as Meta-ICI, using the same full-batch gradient descent update, learning rate, and adaptation-step budget.

### A.2 Pendulum System (Experiment 2)

This experiment evaluates Fast Meta-ICI in the fully observable setting. The benchmark uses a damped nonlinear pendulum with full-state measurements, allowing target adaptation to use scattered one-step transitions. We describe the closed-loop data collection procedure, the shifted test protocol, the validation and reporting rules, and the Schur-Koopman implementation details.

#### A.2.1 System Dynamics and Closed-Loop Data Collection

We use a damped nonlinear pendulum as the fully observable benchmark. Pendulum systems are standard nonlinear mechanical benchmarks in dynamics and control because the restoring term $sin(\theta)$ induces strong state-dependent nonlinearity while the model remains low-dimensional and interpretable (Boubaker, 2013; Strogatz, 2024). The dynamics of the damped nonlinear pendulum with state $x = [\theta, \omega]^\top$ and scalar input $u$ is given as follows:

$$\dot{\theta} = \omega, \qquad \dot{\omega} = -\Omega^2 \sin(\theta) - 2\zeta\Omega\omega + u.$$

The target system uses $\zeta = 0.1$ and $\Omega = 2.0$. All trajectories are simulated with RK4 integration and a time step of $\Delta t = 0.05$. The closed-loop data are generated using a negative-feedback adaptive PD controller

$$u_t = r_t - K(x_t), \qquad K(x_t) = (2\Omega + 1)\theta_t + 2\zeta\omega_t.$$

For the target system parameters, this yields $K(x_t) = 5\theta_t + 0.2\omega_t$. Observation noise is zero-mean Gaussian noise with standard deviation 0.01, truncated at $\pm 0.03$.

**Training excitation.** Both target-system full-data training and meta-training use randomized bounded multisine references. Each reference is synthesized from 30 sinusoidal components with frequencies uniformly covering 0.5–10 Hz, random phases, and trajectory-wise random amplitude bounds. The target full-data set contains 1600 trajectories of length 50; the sequence loss during full-data training uses a horizon of 10. For meta-training, we sample 64 tasks with $\zeta \in [0.05, 0.3]$ and $\Omega \in [0.5, 4.5]$. Each task contains 1800 trajectories of length 50. Initial angles are sampled uniformly from $[-3, 3]$ and initial angular velocities are set to zero.

#### A.2.2 Test Protocol and Validation Selection

The test inputs are deliberately different from the multisine training excitation. We evaluate two input families consisting of zero-input free responses and step responses. The zero-input tests use initial angles

$$\theta_0 \in \{0.5, 1.0, 1.8, 2.5, 2.8\}, \qquad \omega_0 = 0,$$

with $r_t = 0$. The step-response tests use $x_0 = 0$ and step amplitudes

$$r_t \in \{0.5, 1.0, 1.8, 2.4, 2.9\}.$$

All reported test rollouts use a horizon of 200 steps.

To avoid selecting checkpoints or adaptation steps on the test set, we use a held-out validation protocol with intermediate zero-input and step-response magnitudes. The validation set contains zero-input tests with $\theta_0 \in \{0.75, 1.5, 2.2\}$ and step-response tests with amplitudes $\{0.75, 1.5, 2.6\}$. All validation rollouts use a horizon of 200 steps. The validation score is the average late-horizon NRMSE over the validation rollouts and over the two state coordinates. Each 200-step rollout is split into four equal segments $Q_1$–$Q_4$, each containing 50 steps. For Fast Meta-ICI, the final test metrics are computed over five independent adaptation-data seeds. For each seed, the model is adapted from $K = 200$ randomly sampled scattered single-step transitions from the target system. For the Full-Data SK-ICI Reference, we train five full-data models and retain the best checkpoint of each seed according to the same validation score, evaluated after every training epoch. For Fast Meta-ICI, each reported table entry is computed by first averaging over the five test scenarios within the same input family, then reporting the mean ± standard deviation over the five adaptation-data seeds. For the Full-Data SK-ICI Reference, the tables report the mean ± standard deviation over the five validation-selected full-data runs.

### A.2.3 Schur-Koopman Architecture and Optimization

The SK model uses a 32-dimensional latent state. The encoder and decoder are three-layer bias-free MLPs with hidden dimension 64 and Tanh activations. The latent dynamics matrix is parameterized through a Schur-style stable linear map with maximum spectral radius 0.99. The control input is injected through a learned bias-free linear map from the scalar input to the two-dimensional state space. The reconstruction loss weight is set to 1.0.

**Full-Data SK-ICI Reference.** The full-data reference model is trained on the target system with Adam, learning rate $10^{-3}$, batch size 256, and 100 epochs. We do not use a fixed final epoch. After every training epoch, we evaluate the model on the held-out validation scenarios and retain the best checkpoint for each training seed. The resulting validation-selected full-data models are used only as an empirical reference under the same SK architecture and evaluation protocol.

**Fast Meta-ICI.** Hybrid MAML uses one inner-loop step, inner-loop learning rate $10^{-3}$, meta learning rate $5\times10^{-4}$, task batch size 32, query batch size 64, and outer-loop rollout horizon 10. The meta-training process runs for up to 30000 outer-loop updates, with coarse validation-based checkpoint selection from checkpoints evaluated every 100 outer-loop updates. Meta-SGD is enabled for the SK Hybrid MAML run, with initial per-parameter learning rate $10^{-3}$ (Li et al., 2017). At each validation point, the current checkpoint is adapted on a fixed validation adaptation set and evaluated across all candidate adaptation steps from 0 to 19. The checkpoint and adaptation step with the lowest validation score are selected before final testing.

**Target adaptation.** Fast Meta-ICI is adapted with the learned Meta-SGD per-parameter learning rates from the selected checkpoint. The selected adaptation step is reused across the five adaptation-data seeds in final testing. For Scratch SK, we first select the adaptation step on the validation set using the same candidate steps from 0 to 19. The selected Scratch SK step is then reused across the five adaptation-data seeds. Under the current configuration, Scratch SK rollouts diverged across seeds and are therefore excluded from the main table.

## B Proof of $\mathcal{L}_p$ Stability for Schur-Koopman Architecture

This section provides the detailed proof of Theorem 1.

Define $z_t = \phi_\theta(x_t)$ and we have:

$$\begin{aligned} z_{t+1} &= \phi_\theta(x_{t+1}) \\ &= \phi_\theta\big(\psi_\theta(A_\theta \phi_\theta(x_t)) + g_\theta(x_t) r_t\big) \\ &= \phi_\theta\big(\psi_\theta(A_\theta z_t) + g_\theta(x_t) r_t\big) \end{aligned} \tag{12}$$

Rewrite equation 12 as:

$$\begin{aligned} z_{t+1} &= \phi_\theta\big(\psi_\theta(A_\theta z_t)\big) + \Big[\phi_\theta\big(\psi_\theta(A_\theta z_t) + g_\theta(x_t) r_t\big) - \phi_\theta\big(\psi_\theta(A_\theta z_t)\big)\Big] \\ &= F(z_t) + w_t \end{aligned} \tag{13}$$

where $w_t = \phi_\theta\big(\psi_\theta(A_\theta z_t) + g_\theta(x_t) r_t\big) - \phi_\theta\big(\psi_\theta(A_\theta z_t)\big)$.

According to the Lipschitz of $\phi$, we have

$$\|w_t\|_2 \leq L_\phi \|g_\theta(x_t) r_t\|_2 \leq L_\phi M \|r_t\|_2$$

and by the norm equivalence, we can get

$$\|w_t\|_P \leq c_2 \|w_t\|_2 \leq c_2 L_\phi M \|r_t\|_2$$

where $c_2 > 0$.

With equation 13, we have:

$$\|z_{t+1}\|_P \leq \lambda \|z_t\|_P + \|w_t\|_P \tag{14}$$

Expanding the inequality 14, we have:

$$\|z_t\|_P \leq \sum_{k=0}^{t-1} \lambda^{t-1-k} \|w_k\|_P$$

By Young's inequality for convolution, we have:

$$\|\boldsymbol{z}\|_{\ell_p,P} \leq \frac{1}{1-\lambda} \|\boldsymbol{w}\|_{\ell_p,P} \leq \frac{c_2 L_\phi M}{1-\lambda} \|\boldsymbol{r}\|_{\ell_p} \tag{15}$$

where $\|\boldsymbol{z}\|_{\ell_p,P} = \|(\|z_0\|_P, \|z_1\|_P, ...)\|_{\ell_p}$.

Applying the Euclidean norm to both sides of equation 8, we have:

$$\begin{aligned} \|x_{t+1}\|_2 &\leq L_\psi \|A_\theta z_t\|_2 + M \|r_t\|_2 \\ &\leq \frac{L_\psi \|A_\theta\|_2}{c_1} \|z_t\|_P + M \|r_t\|_2 \end{aligned}$$

where $c_1 > 0$.

Let $\nu = \frac{L_\psi \|A_\theta\|_2}{c_1}$. Therefore, we have:

$$\left(\sum_{t=0}^{\infty} \|x_{t+1}\|_2^p\right)^{1/p} \leq \left(\sum_{t=0}^{\infty} (\nu \|z_t\|_P + M \|r_t\|_2)^p\right)^{1/p}$$

By Minkowski's Inequality, we have:

$$\left(\sum_{t=0}^{\infty} (\nu \|z_t\|_P + M \|r_t\|_2)^p\right)^{1/p} \leq \left(\sum_{t=0}^{\infty} (\nu \|z_t\|_P)^p\right)^{1/p} + \left(\sum_{t=0}^{\infty} (M \|r_t\|_2)^p\right)^{1/p}$$

Therefore, we have

$$\|\boldsymbol{x}\|_{\ell_p} \leq \nu \|\boldsymbol{z}\|_{\ell_p,P} + M \|\boldsymbol{r}\|_{\ell_p} \tag{16}$$

Substituting equation 15 into equation 16, we have:

$$\|\boldsymbol{x}\|_{\ell_p} \leq \left(\frac{c_2 \nu L_\phi M}{(1-\lambda)} + M\right) \|\boldsymbol{r}\|_{\ell_p}$$

Let $C = \frac{c_2 \nu L_\phi M}{(1-\lambda)} + M$. Obviously, $C > 0$, and therefore we have:

$$\|\boldsymbol{x}\|_{\ell_p} \leq C \|\boldsymbol{r}\|_{\ell_p}$$